High-Throughput Screening of High Entropy Spinel Electrolytes for Multivalent Batteries

Mahesh J Dheerasinghe[a+], Yi Gan[b+], Lin Wang[a], Yufang He[a], Zhengda He[a], Gui-Liang Xu[c], Yang Zhao[b*] and Bin Ouyang[a*]

Electronic Supplementary Information (ESI)

Supporting note 1. Computational Methods

Density Function Theory (DFT) energy calculations were performed on the target compounds using the Vienna Ab initio Simulation Package (VASP)[1, 2] and the projector-augmented wave (PAW)[3, 4] method, incorporating spin polarization. Structural relaxation was conducted in a two-step process. In the first step, a coarse k-point sampling was employed using VASP's fully automatic k-point generation scheme with a length parameter of $R_k = 1$. This was followed by a finer k-point mesh in the second step, using $R_K = 25$, to ensure accurate Brillouin zone integration. The electronic self-consistent field (SCF) convergence criterion was set to 1×10^{-4} eV, and the plane-wave energy cutoff was fixed at 520 eV.[5]

The entries retrieved from the Materials Project[6] were filtered based on an energy cutoff (energy above hull ranging from 0.0 to 0.01 eV) and were calculated using both GGA and GGA+U to ensure consistency in the results. Additionally, the DFT total energy was recalculated for the competing phases to maintain consistent simulation parameters between the target compounds and competing phases.

Supporting note 2. Competing Phases

Table S1. Competing phases of first 5 lowest E_{hull} target compositions of Mg-based spinels.

No.	Compound	Competing Phases with coefficient
1	Mg2(ZnMgGaSb)O8	Sb2Mg4O9: 0.54; ZnGa2O4: 0.250; ZnO: 0.07; MgO: 0.14
2	Mg2(ZnMgInSb)O8	ZnO: 0.14; MgO: 0.14; Sb2Mg4O9: 0.54; In2O3: 0.18
3	Mg2(AlMgGaSn)O8	SnMg2O4: 0.50; MgGa2O4: 0.25; MgAl2O4: 0.25
4	Mg2(InMgGaSn)O8	SnMg2O4: 0.50; MgGa2O4: 0.25; In2O3: 0.18; MgO: 0.07
5	Mg2(ScMgZnSb)O8	Sb2Mg4O9: 0.54; MgO: 0.14; Sc2O3: 0.18; ZnO: 0.14

Table S2. Competing phases of first 5 lowest E_{hull} target compositions of Zn-based spinels.

No.	Compound	Competing Phases
1	Zn2(MgZnGaSb)O8	Sb2Mg4O9: 0.18; ZnGa2O4: 0.25; MgSb2O6: 0.21; ZnO: 0.36
2	Zn2(MgZnInSb)O8	Sb2Mg4O9: 0.18; MgSb4O12: 0.21; ZnO: 0.43; In2O3: 0.18
3	Zn2(MgAlGaSn)O8	SnMg2O4: 0.25; ZnO: 0.14; ZnGa2O4: 0.25; ZnAl2O4: 0.25; SnO2: 0.17
4	Zn2(MgInGaSn)O8	ZnO: 0.21; SnMg2O4: 0.25; In2O3: 0.18; ZnGa2O4: 0.25; SnO2: 0.11
5	Zn2(MgAlZnSb)O8	Sb2Mg4O9: 0.18; MgSb2O6: 0.21; ZnAl2O4: 0.25; ZnO: 0.36

Table S3. Competing phases of first 5 lowest E_{hull} target compositions of Ca-based spinels.

No.	Compound	Competing Phases
1	Ca2(MgCaInSb)O8	CaIn2O4: 0.25; Ca2Sb2O7: 0.39; MgO: 0.14; CaO: 0.21
2	Ca2(ZrCaScIn)O8	CaIn2O4: 0.25; CaZrO3: 0.36; CaSc2O4: 0.25; CaO: 0.14
3	Ca2(ZnCaInSb)O8	CaIn2O4: 0.25; Ca2Sb2O7: 0.39; ZnO: 0.14; CaO: 0.21
4	Ca2(HfCaScIn)O8	CaIn2O4: 0.25; CaHfO3: 0.36; CaSc2O4: 0.25; CaO: 0.14
5	Ca2(ScCaInSn)O8	Ca2SnO4: 0.50; CaIn2O4: 0.25; CaSc2O4: 0.25

Supporting note 3. Energy Above Hull values.

Table S4. The lowest five energy above hull and entropy stabilization temperatures of Mg-based spinels.

No.	**Compound**	**Energy Above Hull (meV/atom)**	**Entropy Stabilization Temperature (K)**
1	Mg2(ZnMgGaSb)O8	8.139	238.47
2	Mg2(ZnMgInSb)O8	15.724	460.69
3	Mg2(AlMgGaSn)O8	22.322	653.99
4	Mg2(InMgGaSn)O8	22.352	654.88
5	Mg2(ScMgZnSb)O8	23.075	676.04

Table S5. The lowest five energy above hull and entropy stabilization temperatures of Zn-based spinels.

No.	**Compound**	**Energy Above Hull (meV/atom)**	**Entropy Stabilization Temperature (K)**
1	Zn2(MgZnGaSb)O8	0.262	7.67
2	Zn2(MgZnInSb)O8	9.526	279.08
3	Zn2(MgAlGaSn)O8	12.890	377.66
4	Zn2(MgInGaSn)O8	14.292	418.72
5	Zn2(MgAlZn2Sb)O8	17.298	506.80

Table S6. The lowest five energy above hull and entropy stabilization temperatures of Ca-based spinels.

No.	**Compound**	**Energy Above Hull (meV/atom)**	**Entropy Stabilization Temperature (K)**
1	Ca2(MgCaInSb)O8	24.259	710.73

2	Ca2(ZrCaScIn)O8	32.336	947.38
3	Ca2(ZnCaInSb)O8	32.488	951.83
4	Ca2(HfCaScIn)O8	35.589	1042.69
5	Ca2(ScCaInSn)O8	36.127	1058.45

Supporting note 4. The relationship between X and r_{ion} of octahedral site elements.

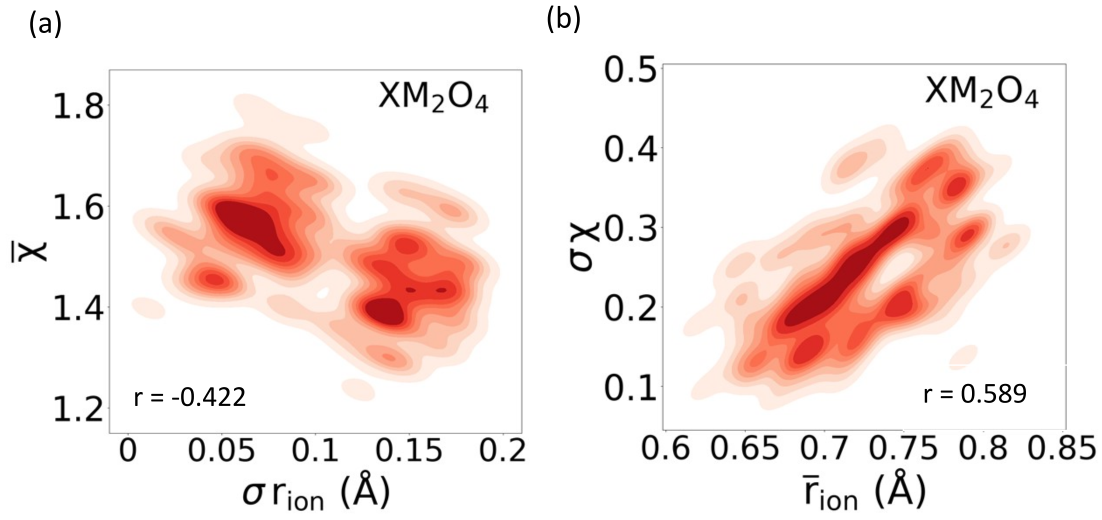

Figure S1: (a) Relationship between and of octahedral-site elements. (b) Relationship between σ χ and of octahedral-site elements. “X” represents Mg/Zn/Ca and “r” represent the Pearson correlation coefficient.

The cation combinations at the octahedral sites are identical across all three spinel types; therefore, they exhibit similar trends in key structural descriptors. Specifically, the average electronegativity ($\bar{\chi}$) and the standard deviation of the ionic radius ($\sigma\ r_{ion}$) of the octahedral-site elements show a negative correlation, with a Pearson correlation coefficient of –0.422. In contrast, the standard deviation of electronegativity (σ χ) and the average ionic radius ($\bar{r}_{ion}$) of the octahedral-site elements exhibit a positive correlation, with a Pearson correlation coefficient of 0.589. These consistent relationships underscore the influence of octahedral-site chemistry on the observed descriptor trends across the spinel systems.

Supporting note 5. Material Synthesis and Characterization

All of the Spinel SSEs products were synthesized by using the solid-state reaction method.[2] $Mg(OH)_2$ (Sigma-Aldrich, 99%), $CaCO_3$ (Themo Fisher Scientific, 99.95%), ZnO (Themo Fisher Scientific, 99.99%), MgO (Sigma-Aldrich, 99.99%), Ga_2O_3 (Themo Fisher Scientific, 99.999%), Sb_2O_5, (Themo Fisher Scientific, 99.998%), In_2O_3 (Themo Fisher Scientific, 99.99%) were used as the precursors. All the calculated materials were mixed in ethanol and then put into a 100 mL zirconia ball milling jar with five zirconia balls using a Retsch PM 200 planetary ball mill at 250 RPM for 12 h. The precursors were then dried overnight in an oven at 75 °C before being pelletized. The precursor pellets were first calcinated in the air at 330 °C for 8 hours and then naturally cooled to RT. After the calcination, the pellets were ground into powders by using PM 200 under 550 RPM for 1 hour. The resulting powders were pelletized and sintered in the air again at 1,050 °C for 10 hours to densify the pellets. Lab-based Powder X-ray diffraction (XRD) spectrums were measured by the Bruker AXS D8 Advance with Cu Kα radiation (λ = 1.5406Å) source.

References

(1) Kresse, G.; Furthmüller, J. Efficiency of ab-initio total energy calculations for metals and semiconductors using a plane-wave basis set. *Computational materials science* **1996**, *6* (1), 15-50.

(2) Chen, Y.; Lun, Z.; Zhao, X.; Koirala, K. P.; Li, L.; Sun, Y.; O'Keefe, C. A.; Yang, X.; Cai, Z.; Wang, C. Unlocking Li superionic conductivity in face-centred cubic oxides via face-sharing configurations. *Nature Materials* **2024**, *23* (4), 535-542.

(3) Kresse, G.; Joubert, D. From ultrasoft pseudopotentials to the projector augmented-wave method. *Physical review b* **1999**, *59* (3), 1758.

(4) Perdew, J. P.; Burke, K.; Ernzerhof, M. Generalized gradient approximation made simple. *Physical review letters* **1996**, *77* (18), 3865.

(5) Kresse, G.; Furthmüller, J. Efficient iterative schemes for ab initio total-energy calculations using a plane-wave basis set. *Physical review B* **1996**, *54* (16), 11169.

(6) Ong, S. P.; Richards, W. D.; Jain, A.; Hautier, G.; Kocher, M.; Cholia, S.; Gunter, D.; Chevrier, V. L.; Persson, K. A.; Ceder, G. Python Materials Genomics (pymatgen): A robust, open-source python library for materials analysis. *Computational Materials Science* **2013**, *68*, 314-319.